ChemComm

COMMUNICATION

View Article Online
View Journal | View Issue

Published on 16 November 2015. Downloaded by Universiteit van Amsterdam on 08/01/2016 07:19:53.

Cite this: *Chem. Commun.*, 2016, 52, 1166

Received 1st October 2015,
Accepted 16th November 2015

DOI: 10.1039/c5cc08210b

www.rsc.org/chemcomm

High acetylene/ethylene separation in a microporous zinc(II) metal–organic framework with low binding energy†

Hui-Min Wen,[a] Bin Li,*[a] Hailong Wang,[a] Rajamani Krishna[b] and Banglin Chen*[a]

A novel zinc(II) metal–organic framework UTSA-67a with narrow one-dimensional (1D) pore channels and inner cages of moderate size has been developed for highly selective separation of C_2H_2/C_2H_4 mixtures at room temperature.

The removal of acetylene from acetylene/ethylene mixtures (1/99) is an industrially important task given the fact that pure ethylene has been widely utilized for the production of polymers and other useful chemicals. During steam cracking of ethane to produce ethylene in industry, a small amount of acetylene (typically 1%) is unavoidably generated as one of the by-products. Because acetylene has a deleterious effect on end-products of ethylene such as polyethene, it is necessary to remove acetylene from crude ethylene to the acceptable level of no more than 40 ppm of impurity. The commercial technologies for the removal of acetylene include partial hydrogenation and solvent extraction, which are high cost and energy-intensive.[1] One alternative energy-efficient strategy is the adsorptive separation technology which is based on the selective adsorption of porous materials for acetylene and ethylene. The development of new porous materials is the key to implement this adsorptive technology for this important industrial separation.

The last two decades have witnessed the emergence of porous metal–organic frameworks (MOFs), which can be straightforwardly self-assembled from metal ions/clusters and organic linkers. They have become very promising candidates for gas storage and separation.[2,3] The richness of metal ions/clusters and organic linkers has enabled us to rationally tune and predesign their structures, pore/window sizes, and functionalities for the separation of some specific gas molecules.[4] Recently, microporous MOFs have been of great interest as promising candidates for the separation of light hydrocarbons.[5–9] Among the diverse gas separations, MOFs for the separation of C_2H_2/C_2H_4 have been very challenging and not fully explored because of their similar sizes, volatilities, and electronic structures of C_2H_2/C_2H_4.[5c] Nowadays two types of MOFs have been realized for this important separation: (a) those with small pore windows and thus sieving effects as exemplified in mixed MOFs (M'MOFs) series[10,11] and (b) those with specific open metal sites as indicated in MOF-74 series.[12,13] Despite high selectivities for C_2H_2/C_2H_4 separation, those M'MOFs exhibit extraordinarily low C_2H_2 uptake capacities due to their narrow pore windows. In contrast, high densities of open metal sites within the MOF-74 series can notably enhance their C_2H_2 uptake capacities; however, their large pores lead to quite low selectivities.[12] Furthermore, the high densities of open metal sites also result in a strong binding energy for C_2H_2 molecules and thus significantly high regeneration energy costs. Therefore, an ideal MOF for this challenging separation should not only have narrow pore channels to maximize the sieving effects for achieving high separation selectivity, but also have inner cages of moderate size to improve C_2H_2 uptake capacity. Very recently, our group has realized a very promising MOF UTSA-100, whose pore structures almost meet the above criteria, which exhibits the best performance so far for the removal of acetylene from 1% acetylene/ethylene mixtures.[15] This encourages us to seek new MOF materials that have similar structures for highly efficient C_2H_2/C_2H_4 separation.

With this goal in our mind, we reported herein the synthesis of a novel porous MOF (termed as UTSA-67) by making use of a new tetracarboxylate ligand whose structural features indeed meet the above-mentioned criteria: narrow 1D pore channels with 3.3 Å diameter for their high C_2H_2/C_2H_4 sieving effects, moderate inner cages of 7 Å for high C_2H_2 uptake capacity, and low binding energy due to the absence of open metal sites. As expected, the C_2H_2/C_2H_4 separation selectivity of UTSA-67a is comparable to that of UTSA-100a, and three times higher than

[a] *Department of Chemistry, University of Texas at San Antonio, One UTSA Circle, San Antonio, Texas 78249-0698, USA. E-mail: bin.li@utsa.edu, banglin.chen@utsa.edu; Fax: +1-210-458-7428*

[b] *Van 't Hoff Institute for Molecular Sciences, University of Amsterdam, Science Park 904, 1098 XH Amsterdam, The Netherlands*

† Electronic supplementary information (ESI) available: Synthesis and characterization of UTSA-67, PXRD, TGA, sorption isotherms, and breakthrough simulations. CCDC 1425153. For ESI and crystallographic data in CIF or other electronic format see DOI: 10.1039/c5cc08210b

This journal is © The Royal Society of Chemistry 2016

Published on 16 November 2015. Downloaded by Universiteit van Amsterdam on 08/01/2016 07:19:53.

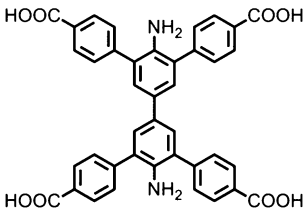

Scheme 1 Schematic structure of the new organic ligand (H_4L) that serves as a linker in UTSA-67.

those of the MOF-74 series. The inner cages of moderate size within UTSA-67a can notably improve the C_2H_2 uptake capacity.[16] Most importantly, the absence of open metal sites within UTSA-67a results in the very low binding energy and thus low regeneration energy costs, which are much lower than those of most of the examined MOFs. Taking these results together, UTSA-67a is indeed among the best materials for the selective removal of acetylene from ethylene/acetylene mixtures.

The organic linker (H_4L, Scheme 1) was simply prepared through the Suzuki cross-coupling reaction of 3,3′,5,5′-tetrabromo-benzidine with 4 equiv. of 4-methoxycarbonylphenylboronic acid, followed by hydrolysis and acidification. Reactions of the organic linker and $Zn(NO_3)_2{\cdot}6H_2O$ in DMF–EtOH at 80 °C for 24 h afforded yellow block crystals. Based on single-crystal XRD studies, TGA and elemental analysis, the as-synthesized UTSA-67 can be formulated as $[Zn_2L]{\cdot}2DMF{\cdot}4H_2O$. The phase purity of the bulk material was independently confirmed by powder X-ray diffraction (Fig. S3, ESI†).

Single-crystal X-ray diffraction analysis reveals that UTSA-67 adopts a three-dimensional network that crystallizes in a hexagonal space group $P6_522$. As shown in Fig. S5 (ESI†), each organic linker contains two bridging carboxylates, two monodentate carboxylates and two coordinated amino groups. The secondary building unit (SBU) is a binuclear zinc cluster in which two equivalent Zn1 atoms are coordinated by two amino groups and four carboxylate groups from six different ligands with a Zn1···Zn1 distance of 3.702(1) Å (Fig. 1a). Topologically, each binuclear zinc cluster and each organic linker can be regarded as 6-connected nodes, which are linked with each other to form a (6,6)-connected network with the nia topology. There exist one-dimensional open channels of about 3.3 Å in diameter along the *c* axis (Fig. 1b), while no channels along the *a* and *b* axes (Fig. 1c). To our surprise, there are a lot of inner cages of moderate size around the 1D pore channels (Fig. 1d), which can be used to improve the high C_2H_2 uptake. These unique pore structures of UTSA-67 suggest its great potential for selective adsorptive separation of C_2H_2–C_2H_4 mixtures.

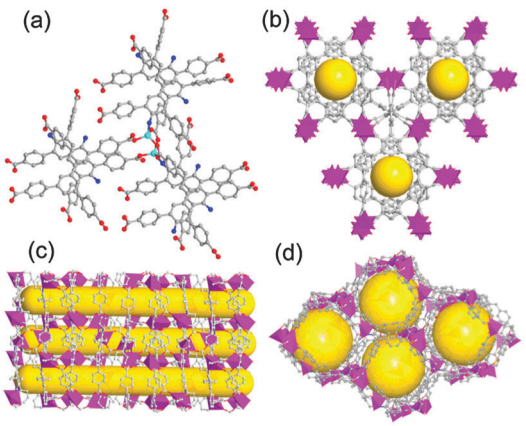

Fig. 1 X-ray single crystal structure of UTSA-67 indicating (a) the binuclear zinc–carboxylate unit linked by six organic ligands; (b) the pore channels viewed along the *c* axes; (c) viewed along the *a* and *b* axes; (d) the inner cages of about 7 Å in diameter along the *c* axes. All hydrogen atoms have been omitted for clarity. Cyan, blue, red, and gray spheres represent Zn, N, O, and C atoms, respectively.

Prior to gas adsorption measurements, the as-synthesized UTSA-67 was solvent-exchanged with dry acetone, and then evacuated at 273 K for 36 h and at room temperature for an additional 24 h under high vacuum to yield the activated UTSA-67a. As shown in Fig. S6 (ESI†), the permanent porosity of UTSA-67a was unambiguously established by nitrogen sorption at 77 K. The N_2 sorption isotherm at 77 K exhibits a typical Type-I sorption behaviour, characteristic of a microporous material, with an N_2 uptake of 302.68 $cm^3\ g^{-1}$. The Brunauer–Emmett–Teller (BET) surface area and pore volume were estimated to be 1137 $m^2\ g^{-1}$ and 0.47 $cm^3\ g^{-1}$, respectively.

The unique pore structure and permanent microporosity in UTSA-67a motivated us to examine its potential applications for the industrially important C_2H_2/C_2H_4 separation. We first collected the single-component adsorption isotherms for acetylene and ethylene up to 1 atm at 296 K, respectively. Due to the large cages around the 1D pore channels, UTSA-67a can take up a high amount of C_2H_2 (116 $cm^3\ g^{-1}$) at 1 atm and 296 K (Fig. 2), which is much higher than that of some of the promising MOFs, such as M'MOF-3a, UTSA-100a, and UTSA-60a[7a] (Table 1). However, a much lower C_2H_4 uptake (63 $cm^3\ g^{-1}$, at 296 K and 1 bar) was observed for UTSA-67a, attributable to the extremely small 1D pore channels of 3.3 Å.[10] The C_2H_2/C_2H_4 uptake ratio of UTSA-67a was estimated to be 1.84 (Table 1), which is notably higher than the MOF-74 series (1.11–1.16) and NOTT-300 (1.48). Both the relatively high C_2H_2 uptake and C_2H_2/C_2H_4 uptake ratio of UTSA-67a further prompted us to investigate its feasibility to selectively separate C_2H_2 from binary C_2H_2/C_2H_4 mixtures.

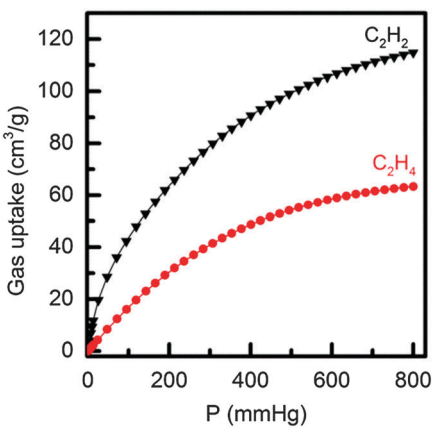

Fig. 2 Single-component adsorption isotherms for C_2H_2 (black) and C_2H_4 (red) of UTSA-67a at 296 K.

Published on 16 November 2015. Downloaded by Universiteit van Amsterdam on 08/01/2016 07:19:53.

Table 1 Comparison of some microporous MOFs for C_2H_2/C_2H_4 separation at room temperature

	UTSA-67a	M'MOF-3a	FeMOF-74	NOTT-300	UTSA-100a
Surface area[a] ($m^2\ g^{-1}$)	1137	110	1350	1370	970
Pore volume ($cm^3\ g^{-1}$)	0.47	0.165	0.626	0.433	0.399
Size of pore window (Å)	3.3 × 3.3	3.4 × 4.8	11 × 11	6.5 × 6.5	4.3 × 4.3
C_2H_2 uptake (mmol g^{-1})	5.13	1.90	6.80	6.34[b]	4.27
C_2H_4 uptake (mmol g^{-1})	2.81	0.40	6.10	4.28[b]	1.66
C_2H_2/C_2H_4 uptake ratio	1.84	4.75	1.11	1.48	2.57
Selectivity[c]	5–6	24.03	2.08	2.17	5–10.7
Ref.	This work	13	13	14	14

[a] BET. [b] At a temperature of 293 K. [c] IAST analysis for C_2H_2/C_2H_4 mixtures containing 1% acetylene at 100 kPa.

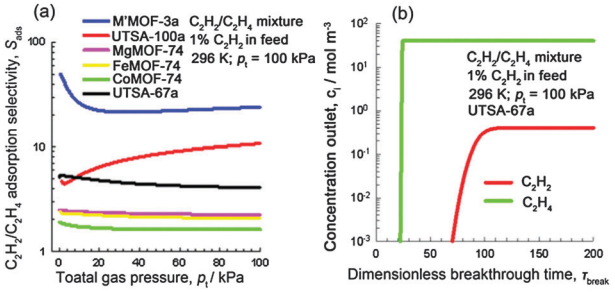

Fig. 3 (a) IAST calculations of C_2H_2/C_2H_4 adsorption selectivities for UTSA-67a and other examined MOFs at 296 K. (b) Transient breakthrough of C_2H_2/C_2H_4 mixture containing 1% C_2H_2 mixture in an adsorber bed packed with UTSA-67a. The total bulk gas phase is at 296 K and 100 kPa. The partial pressures of C_2H_2 and C_2H_4 in the inlet feed gas mixture are, respectively, p_1 = 1 kPa and p_2 = 99 kPa. For the breakthrough simulations, the following parameter values were used, as before, L = 0.12 m; ε = 0.75; and u = 0.00225 m s^{-1}.

We utilized Ideal Adsorbed Solution Theory (IAST) to calculate the adsorption selectivity of UTSA-67a for the binary C_2H_2/C_2H_4 mixture containing 1% C_2H_2. Fig. 3a makes a comparison of the adsorption selectivity of the C_2H_2/C_2H_4 mixture (1 : 99, v/v) as a function of total bulk gas phase pressure between UTSA-67a and other well-known porous MOFs at 296 K. It can be seen that the initial adsorption selectivity of UTSA-67a lies in the range of 5–6 at room temperature. This value is comparable to that of UTSA-100a (the best reported MOF so far for C_2H_2/C_2H_4 separation through a breakthrough and/or fixed bed) and almost three times higher than those obtained for the MOF-74 series and NOTT-300. This is really remarkable, making UTSA-67a one of the promising MOFs with high adsorption selectivities for C_2H_2/C_2H_4 separation. Fig. S9 (ESI†) compares the gravimetric uptake capacities of C_2H_2 for adsorption from mixtures containing 1% C_2H_2. At a total gas phase pressure of 100 kPa, UTSA-67a shows a comparatively high uptake capacity, which is comparable to FeMOF-74 and CoMOF-74, but higher than NOTT-300 and M'MOF-3a.[14] As a result, the combined features of high adsorption selectivity and C_2H_2 uptake capacity for UTSA-67a once again highlight its promising potential for highly selective adsorptive separation of C_2H_2–C_2H_4 mixtures.

In order to further prove the feasibility, we performed transient breakthrough simulations using the methodology described in previous literature (ESI†).[15] Fig. 3b shows the concentrations of C_2H_2/C_2H_4 exiting the adsorber packed with UTSA-67a as a function of the dimensionless time, τ, at a total pressure of 1 bar and a temperature of 296 K. We found that the ethylene gas broke through first due to its lower adsorptivity relative to acetylene. There was a significant time interval between the breakthrough of C_2H_2 and C_2H_4, indicating that UTSA-67a can efficiently separate C_2H_2 from the C_2H_2/C_2H_4 (1/99) mixture at room temperature. The breakthrough time, τ_{break} of UTSA-67a, corresponding to the exit gas containing 40 ppm C_2H_2, can be determined from Fig. S10 (ESI†). During the time interval 0–τ_{break}, pure C_2H_4 can be collected, which can satisfy the feedstock requirements of polymerization reactors in the polymer industry. Table S4 (ESI†) presents a comparison of the amount of C_2H_2 captured plotted as a function of the time interval break, where the C_2H_2 capture capacity of UTSA-67a is comparable to the MOF-74 series, but higher than M'MOF-3, NOTT-300, and UTSA-60a.

During industrial practice, when the impurity level exceeds the desired purity level of no more than 40 ppm (indicated by the dashed line in Fig. S10, ESI†) after a certain time, τ_{break}, the adsorption cycle needs to be terminated, so the regeneration process can be initiated. As a result, the regeneration energy cost of a fixed bed is another very important factor that needs to be considered. Fig. 4 presents a comparison of the heats of adsorption (Q_{st}) of C_2H_2 in UTSA-67a with other examined MOFs. Based on the Clausius–Clapeyron equation, the initial Q_{st} of UTSA-67a was calculated to be 32 KJ mol^{-1}, which was rapidly decreased to 20 KJ mol^{-1} with the increasing C_2H_2 loading. We found that the values of Q_{st} in MOFs without open

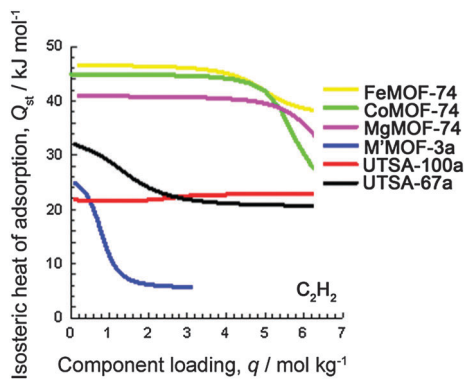

Fig. 4 Comparison of the heats of adsorption (Q_{st}) of C_2H_2 in various MOFs.

 This journal is © The Royal Society of Chemistry 2016

Published on 16 November 2015. Downloaded by Universiteit van Amsterdam on 08/01/2016 07:19:53.

metal sites, like UTSA-67a, UTSA-100a and M'MOF-3a, are significantly lower than that for MOF-74 series and UTSA-60a[7a] with high densities of open metal sites. It is worth noting that the value of Q_{st} for UTSA-67a is also lower than the best MOF UTSA-100a after the C_2H_2 loading exceeded 2.6 mol kg^{-1}. These results indicate that the energy required for the regeneration of UTSA-67a will be lower than that of MOF-74 series and UTSA-100a, resulting in a significant energy saving. Such exceptionally low binding energy for UTSA-67a was mainly attributed to the absence of both open metal sites and free $-NH_2$ groups within this framework. Thus, only the large aromatic sites of UTSA-67a afford the binding energy to guest molecules. Although M'MOF-3 shows the lowest Q_{st} for C_2H_2, the extremely low C_2H_2 uptake capacity limits its overall performance in C_2H_2/C_2H_4 separation.

In conclusion, we have realized a new porous zinc(II) MOF UTSA-67a with narrow 1D pore channels and inner cages of moderate size for highly selective separation of C_2H_2/C_2H_4 mixtures at room temperature. This material exhibits not only high C_2H_2/C_2H_4 separation selectivity but also significantly high C_2H_2 uptake capacity. Such a high separation capacity of UTSA-67a was mainly attributed to extremely narrow pore channels for an extensive sieving effect and inner cages of moderate size to take up the high C_2H_2 amount. The breakthrough simulations further demonstrate the feasibility of UTSA-67a in the removal of acetylene from acetylene/ethylene mixtures containing 1% acetylene. Most importantly, the absence of both open metal sites and free $-NH_2$ groups within UTSA-67a results in its exceptionally low binding energy for C_2H_2 adsorption, thus leading to a significant energy saving.

This work was supported by an award AX-1730 from the Welch Foundation (BC).

Notes and references

1 (*a*) N. A. Khan, S. Shaikhutdinov and H.-J. Freund, *Catal. Lett.*, 2006, **108**, 159; K. Weissermel and H.-J. Arpe, *Industrial Organic Chemistry*, Wiley-VCH, Weinheim, 4th edn, 2003, p. 91.
2 (*a*) H. Furukawa, K. E. Cordova, M. O'Keeffe and O. M. Yaghi, *Science*, 2013, **341**, 6149; (*b*) K. Sumida, D. L. Rogow, J. A. Mason, T. M. McDonald, E. D. Bloch, Z. R. Herm, T.-H. Bae and J. R. Long, *Chem. Rev.*, 2012, **112**, 724; (*c*) S. Furukawa, J. Reboul, S. Diring, K. Sumida and S. Kitagawa, *Chem. Soc. Rev.*, 2014, **43**, 5700; (*d*) Y. He, W. Zhou, G. Qian and B. Chen, *Chem. Soc. Rev.*, 2014, **43**, 5657.
3 (*a*) J.-R. Li, J. Sculley and H.-C. Zhou, *Chem. Rev.*, 2012, **112**, 869; (*b*) P. Nugent, Y. Belmabkhout, S. D. Burd, A. J. Cairns, R. Luebke, K. Forrest, T. Pham, S. Ma, B. Space, L. Wojtas, M. Eddaoudi and M. J. Zaworotko, *Nature*, 2013, **495**, 80; (*c*) O. Shekhah, Y. Belmabkhout, Z. Chen, V. Guillerm, A. Cairns, K. Adil and M. Eddaoudi, *Nat. Commun.*, 2014, **5**, 4228; (*d*) Z. Zhang, Z. Yao, S. Xiang and B. Chen, *Energy Environ. Sci.*, 2014, **7**, 2868; (*e*) B. Li, H.-M. Wen, W. Zhou and B. Chen, *J. Phys. Chem. Lett.*, 2014, **5**, 3468.
4 (*a*) M. Li, D. Li, M. O'Keeffe and O. M. Yaghi, *Chem. Rev.*, 2014, **114**, 1343; (*b*) Y. He, B. Li, M. O'Keeffe and B. Chen, *Chem. Soc. Rev.*, 2014, **43**, 5618; (*c*) B. Li, M. Chrzanowski, Y. Zhang and S. Ma, *Coord. Chem. Rev.*, 2015, DOI: 10.1016/j.ccr.2015.05.005.
5 (*a*) Z. R. Herm, E. D. Bloch and J. R. Long, *Chem. Mater.*, 2014, **26**, 323; (*b*) H. Wu, Q. Gong, D. H. Olson and J. Li, *Chem. Rev.*, 2012, **112**, 836; (*c*) Y. He, W. Zhou, R. Krishnad and B. Chen, *Chem. Commun.*, 2012, **48**, 11813.
6 (*a*) P.-Q. Liao, D.-D. Zhou, A.-X. Zhu, L. Jiang, R.-B. Lin, J.-P. Zhang and X.-M. Chen, *J. Am. Chem. Soc.*, 2012, **134**, 17380; (*b*) Z. R. Herm, B. M. Wiers, J. A. Mason, J. M. V. Baten, M. R. Hudson, P. Zajdel, C. M. Brown, N. Masciocchi, R. Krishna and J. R. Long, *Science*, 2013, **340**, 960; (*c*) N. Nijem, H. Wu, P. Canepa, A. Marti, J. K. J. Balkus, T. Thonhauser, J. Li and Y. J. Chabal, *J. Am. Chem. Soc.*, 2012, **134**, 15201; (*d*) C. Yeon Lee, Y.-S. Bae, N. C. Jeong, O. K. Farha, A. A. Sarjeant, C. L. Stern, P. Nickias, R. Q. Snurr, J. T. Hupp and S. T. Nguyen, *J. Am. Chem. Soc.*, 2011, **133**, 5228; (*e*) G. Chang, M. Huang, Y. Su, H. Xing, B. Su, Z. Zhang, Q. Yang, Y. Yang, Q. Ren, Z. Bao and B. Chen, *Chem. Commun.*, 2015, **51**, 2859.
7 (*a*) H.-M. Wen, B. Li, H. Wang, C. Wu, K. Alfooty, R. Krishna and B. Chen, *Chem. Commun.*, 2015, **51**, 5610; (*b*) H. T. Kwon and H.-K. Jeong, *J. Am. Chem. Soc.*, 2013, **135**, 10763; (*c*) Y.-P. He, Y.-X. Tan and J. Zhang, *Chem. Commun.*, 2013, **49**, 11323; (*d*) J. Jia, L. Wang, F. Sun, X. Jing, Z. Bian, L. Gao, R. Krishna and G. Zhu, *Chem. – Eur. J.*, 2014, **20**, 9073; (*e*) K. Liu, D. Ma, B. Li, Y. Li, K. Yao, Z. Zhang, Y. Han and Z. Shi, *J. Mater. Chem. A*, 2014, **2**, 15823; (*f*) Y.-S. Bae, C. Y. Lee, K. C. Kim, O. K. Farha, P. Nickias, J. T. Hupp, S. T. Nguyen and R. Q. Snurr, *Angew. Chem., Int. Ed.*, 2012, **51**, 1857.
8 S. Yang, A. J. Ramirez-Cuesta, R. Newby, V. Garcia-Sakai, P. Manuel, S. K. Callear, S. I. Campbell, C. C. Tang and M. Schröder, *Nat. Chem.*, 2014, **7**, 121.
9 B. Li, H. Wang and B. Chen, *Chem. – Asian J.*, 2014, **9**, 1474.
10 S. Xiang, Z. Zhang, C.-G. Zhao, K. Hong, X. Zhao, D.-L. Ding, M.- H. Xie, C.-D. Wu, R. Gill, K. M. Thomas and B. Chen, *Nat. Commun.*, 2011, **2**, 204.
11 M. C. Das, Q. Guo, Y. He, J. Kim, C.-G. Zhao, K. Hong, S. Xiang, Z. Zhang, K. M. Thomas, R. Krishna and B. Chen, *J. Am. Chem. Soc.*, 2012, **134**, 8703.
12 E. D. Bloch, W. L. Queen, R. Krishna, J. M. Zadrozny, C. M. Brown and J. R. Long, *Science*, 2012, **335**, 1606.
13 Y. He, R. Krishna and B. Chen, *Energy Environ. Sci.*, 2012, **5**, 9107.
14 T.-L. Hu, H. Wang, B. Li, R. Krishna, H. Wu, W. Zhou, Y. Zhao, Y. Han, X. Wang, W. Zhu, Z. Yao, S. Xiang and B. Chen, *Nat. Commun.*, 2015, **6**, 7328.
15 (*a*) R. Krishna and J. R. Long, *J. Phys. Chem. C*, 2011, **115**, 12941; (*b*) R. Krishna, *Microporous Mesoporous Mater.*, 2014, **185**, 30.
16 S. Xiang, W. Zhou, J. M. Gallegos, Y. Liu and B. Chen, *J. Am. Chem. Soc.*, 2009, **131**, 12415.

Electronic Supplementary Material (ESI) for ChemComm.
This journal is © The Royal Society of Chemistry 2015

Supporting Information

High acetylene/ethylene separation in a microporous zinc(II) metal–organic framework with low binding energy

Hui-Min Wen,[a] Bin Li,*[a] Hailong Wang,[a] Rajamani Krishna,[b] and Banglin Chen*[a]

[a] *Department of Chemistry, University of Texas at San Antonio, One UTSA Circle, San Antonio, Texas 78249-0698, USA. Fax: (+1)-210-458-7428; E-mail: bin.li@utsa.edu; banglin.chen@utsa.edu*

[b] *Van 't Hoff Institute for Molecular Sciences, University of Amsterdam, Science Park 904, 1098 XH Amsterdam, The Netherlands*

1. General Procedures and Materials. All reagents and solvents were commercially available and used without further purification. 4,4′-diaminobiphenyl -3,3′,5,5′-tetrabromide was prepared according to the literature procedure.[1] ^{1}H NMR spectra were recorded on a Varian Mercury 500 MHz spectrometer using tetramethylsilane (TMS) as internal standards. The coupling constants reported in Hertz. FTIR spectra were performed on a Bruker Vector 22 spectrometer at room temperature. The elemental analyses were performed with Perkin–Elmer 240 CHN analyzers. Thermogravimetric analyses (TGA) were carried out using a Shimadzu TGA-50 analyzer under a nitrogen atmosphere with a heating rate of 5 ^{o}C min^{-1}. Powder X–ray diffraction (PXRD) patterns were measured by a Rigaku Ultima IV diffractometer operated at 40 kV and 44 mA with a scan rate of 1.0 deg min^{-1}.

2. Gas sorption Measurements. A Micromeritics ASAP 2020 surface area analyzer was used to measure gas adsorption isotherms. To remove all the guest solvents in the framework, the fresh sample of UTSA-67 was guest–exchanged with dry acetone at least 10 times, filtered and degassed at 273 K for 36 h, and then at 296 K for another 24 hours until the outgas rate was 5 μmHg min^{-1} prior to measurements. The sorption measurement was maintained at 77 K with liquid nitrogen. An ice-water bath (slush) and water bath were used for adsorption isotherms at 273 and 296 K, respectively.

3. Single-crystal X-ray crystallography. The crystal data were collected on an Agilent Supernova CCD diffractometer equipped with a graphite-monochromatic enhanced Cu Kα radiation (λ = 1.54184 Å) at 293 K. The datasets were corrected by empirical absorption correction using spherical harmonics, implemented in the SCALE3 ABSPACK scaling algorithm. The structure was solved by direct methods and refined by full matrix least-squares methods with the SHELX-97 program package.[2] The solvent molecules in the compound are highly disordered. The SQUEEZE subroutine of the PLATON software suit was used to remove the scattering from the highly disordered guest molecules.[3] The resulting new files were used to further refine the structures. The H atoms on C atoms were generated geometrically.

4. Fitting of pure component isotherms

Experimental data on pure component isotherms for C_2H_2, and C_2H_4 in UTSA-67a were measured at temperatures of 273 K and 296 K. The pure component isotherm data for C_2H_2, and C_2H_4 were fitted with the dual-Langmuir-Freundlich isotherm model

$$q = q_{A,sat}\frac{b_A p^{\nu_A}}{1+b_A p^{\nu_A}} + q_{B,sat}\frac{b_B p^{\nu_B}}{1+b_B p^{\nu_B}} \tag{1}$$

with T-dependent parameters b_A, and b_B

$$b_A = b_{A0}\exp\left(\frac{E_A}{RT}\right); \quad b_B = b_{B0}\exp\left(\frac{E_B}{RT}\right) \tag{2}$$

The fitted parameter values are presented in Table S2. The fits are excellent for both components over the entire pressure range.

5. Isosteric heat of adsorption

The isosteric heat of C_2H_2 adsorption, Q_{st}, defined as

$$Q_{st} = RT^2\left(\frac{\partial \ln p}{\partial T}\right)_q \tag{3}$$

was determined using the Clausius-Clapeyron equation by fitting the adsorption isotherms taken at 273 and 296 K to a Langmuir expression. Figure 4 presents a comparison of the heats of adsorption of C_2H_2 in UTSA-67a with five other representative MOFs. We note that values of Q_{st} in UTSA-67a, UTSA-100a and M'MOF-3a are significantly lower than that for MOFs with coordinately unsaturated metal atoms UTSA-60a,[4] FeMOF-74, CoMOF-74, and MgMOF-74. This implies that the regeneration energy requirement of M'MOF-3a, UTSA-67a, and UTSA-100a will be significantly lower than that of UTSA-60, FeMOF-74, CoMOF-74, and MgMOF-74.

6. IAST calculations of adsorption selectivities

The selectivity of preferential adsorption of component *1* over component *2* in a mixture containing *1* and *2*, can be formally defined as

$$S_{ads} = \frac{q_1/q_2}{p_1/p_2} \tag{4}$$

In equation (4), q_1 and q_2 are the absolute component loadings of the adsorbed phase in the mixture. These component loadings are also termed the uptake capacities. We calculate the values of q_1 and q_2 using the Ideal Adsorbed Solution Theory (IAST) of Myers and Prausnitz.[5]

Based on the IAST calculations for C_2H_2/C_2H_4 adsorption selectivities, at a total pressure of 100 kPa, the value of S_{ads} for UTSA-67a is in the range of 5–6, which is comparable to UTSA-100a and UTSA-60a,[4] but much higher than that for NOTT-300 (2.17)[5] and MMOF-74 (in the range of 1.6 to 2.2).

7. Transient breakthrough of C_2H_2/C_2H_4 mixtures in fixed bed adsorbers

The performance of industrial fixed bed adsorbers is dictated by a combination of adsorption selectivity and uptake capacity. For a proper comparison of various MOFs, we perform transient breakthrough simulations using the simulation methodology described in the literature.[6-8] For the breakthrough simulations, the following parameter values were used: framework density, ρ = 1057 kg m^{-3}, length of packed bed, L = 0.12 m; voidage of packed bed, ε = 0.75; superficial gas velocity at inlet, u = 0.00225 m/s. The transient breakthrough simulation results are presented in terms of a *dimensionless* time, τ, defined by dividing the actual time, t, by the characteristic time, $\frac{L\varepsilon}{u}$.

The transient breakthrough simulations in Figure 3b show the concentrations of C_2H_2/C_2H_4 exiting the adsorber packed with UTSA-67a as a function of the dimensionless time, τ. Analogous breakthrough simulations were performed for UTSA-100a, MgMOF-74, FeMOF-74, CoMOF-74, and M'MOF-3a using the isotherm fits parameters that are provided in our earlier work.[8] On the basis of the gas phase concentrations, we can calculate the impurity

level of C_2H_2 in the gas mixture exiting the fixed bed packed with five different MOFs. Figure S10 shows the ppm C_2H_2 in the outlet gas mixture exiting an adsorber packed with UTSA-67a, UTSA-100a, MgMOF-74, FeMOF-74, CoMOF-74, and M'MOF-3a. At a certain time, τ_{break}, the impurity level will exceed the desired purity level of 40 ppm (indicated by the dashed line), that corresponds to the purity requirement of the feed to the polymerization reactor. The adsorption cycle needs to be terminated at that time τ_{break} and the regeneration process needs to be initiated. From a material balance on the adsorber, the amount of C_2H_2 captured during the time interval $0-\tau_{break}$ can be determined. Table 2 provides a summary of the breakthrough times, τ_{break} for various MOFs and the amount of C_2H_2 captured, expressed in mmol per L adsorbent in fixed bed

Figure S11 presents a plot of the amount of C_2H_2 captured plotted as a function of the time interval τ_{break}. The hierarchy of C_2H_2 capture capacities is UTSA-100a > MMOF-74 > UTSA-67a > M'MOF-3a > NOTT-300 > UTSA-60a (Table S4).

Notation

b_A	dual-Langmuir-Freundlich constant for species *i* at adsorption site A, $Pa^{-\nu_i}$
b_B	dual-Langmuir-Freundlich constant for species *i* at adsorption site B, $Pa^{-\nu_i}$
L	length of packed bed adsorber, m
p_i	partial pressure of species *i* in mixture, Pa
p_t	total system pressure, Pa
q_i	component molar loading of species *i*, mol kg^{-1}
q_t	total molar loading in mixture, mol kg^{-1}
q_{sat}	saturation loading, mol kg^{-1}
Q_{st}	isosteric heat of adsorption, J $kmol^{-1}$
t	time, s
T	absolute temperature, K
u	superficial gas velocity in packed bed, m s^{-1}

Greek letters

ε	voidage of packed bed, dimensionless
ν	exponent in dual-Langmuir-Freundlich isotherm, dimensionless
ρ	framework density, kg m^{-3}
τ	time, dimensionless

Subscripts

i	referring to component i
t	referring to total mixture

Scheme S1. Synthetic routes to the organic linker H_4L.

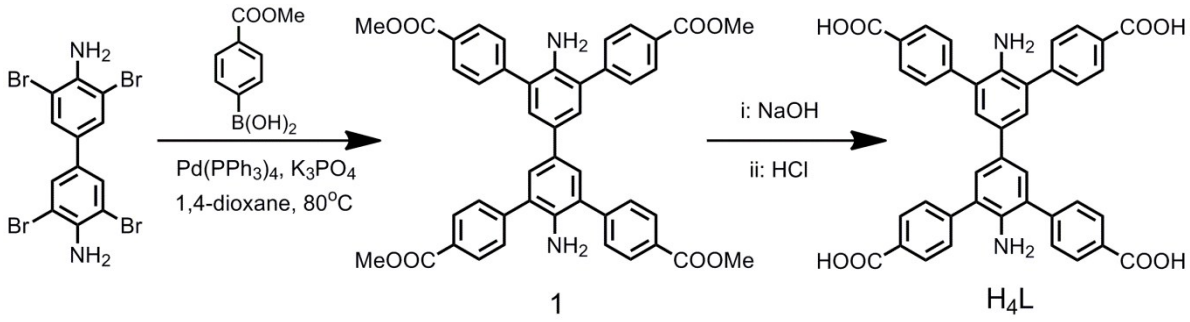

Synthesis of 4,4′-diaminobiphenyl-3,3′,5,5′-tetra-(phenyl-4-carboxylic acid) (H_4L): A mixture of 4,4′-diaminobiphenyl -3,3′,5,5′-tetrabromide (2.48 g, 5 mmol) and 4-methoxycarbonylphenylboronic acid (3.96 g, 22 mmol) were dissolved in dry 1,4-dioxane (80 mL), which was deoxygenated by three freeze-pump-thaw cycles and then protected under N_2 atmosphere. After that, K_3PO_4 (2.55g, 12 mmol) and [$Pd(PPh_3)_4$] (0.3 g, 0.26 mmol) were quickly added to the reaction mixture with stirring and the mixture was heated to 85 ^oC for two days. After cooling down to room temperature, compound 1 was isolated by conventional extraction and procedures. The final product H_4L was obtained by hydrolysis of compound 1 with 2M aqueous NaOH, followed by acidification with concentrated HCl.

Yield: 1.5 g (46%). ^{1}H NMR (500 MHz, d^{6}-DMSO, ppm): δ = 8.04 (d, *J* = 8.10 Hz, 8H), 8.01 (d, *J* = 8.0 Hz, 8H), 7.64 (s, 4H), 6.61 (s, 4H). ^{13}C NMR (d^{6}-DMSO, ppm): δ = 167.61, 143.13, 131.66, 130.46, 130.28, 130.21, 128.92.

Synthesis of UTSA-67. A mixture of the organic linker H_4L (10.0 mg, 0.015 mmol) and $Zn(NO_3)_2{\cdot}6H_2O$ (25.0 mg, 0.084 mmol) was dissolved into a 2.4 mL mixed solvent (DMF/EtOH, 2 mL/0.4 mL) in a screw-capped vial (20 mL). The vial was capped and heated in an oven at 80 °C for 24 h. Dark yellow crystals were obtained by filtration and washed with DMF several times to afford UTSA-67 in 60% yield. UTSA-67 has a best formula as $[Zn_2L]{\cdot}2DMF{\cdot}4H_2O$, which was obtained based on the basis of single-crystal X-ray structure determination, elemental analysis and TGA. Anal. Calcd for $C_{48}H_{50}N_4O_{14}Zn_2$: C, 55.56; H, 4.86; N, 5.40; found: C, 55.37; H, 4.88; N, 5.45. TGA data for loss of 2DMF and $4H_2O$: calcd: 23.80%, found: 23.75%.

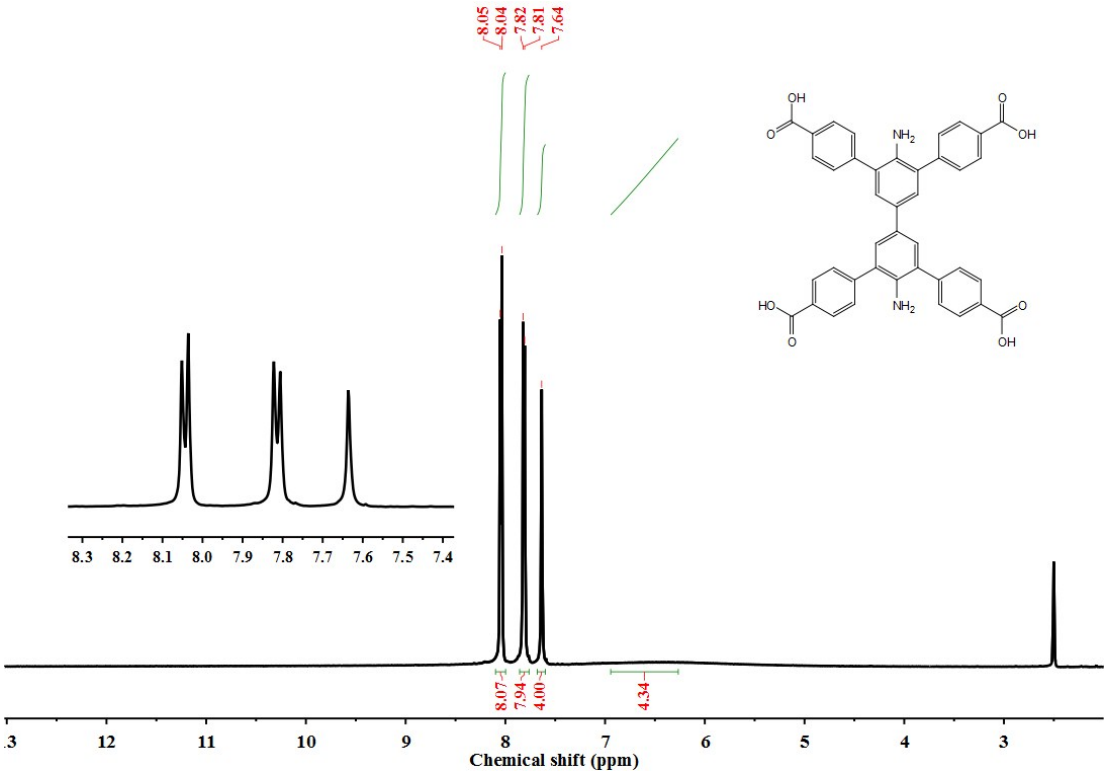

Figure S1. ^{1}H (DMSO-d$_6$, 500MHz) spectra of the ligand H_4L.

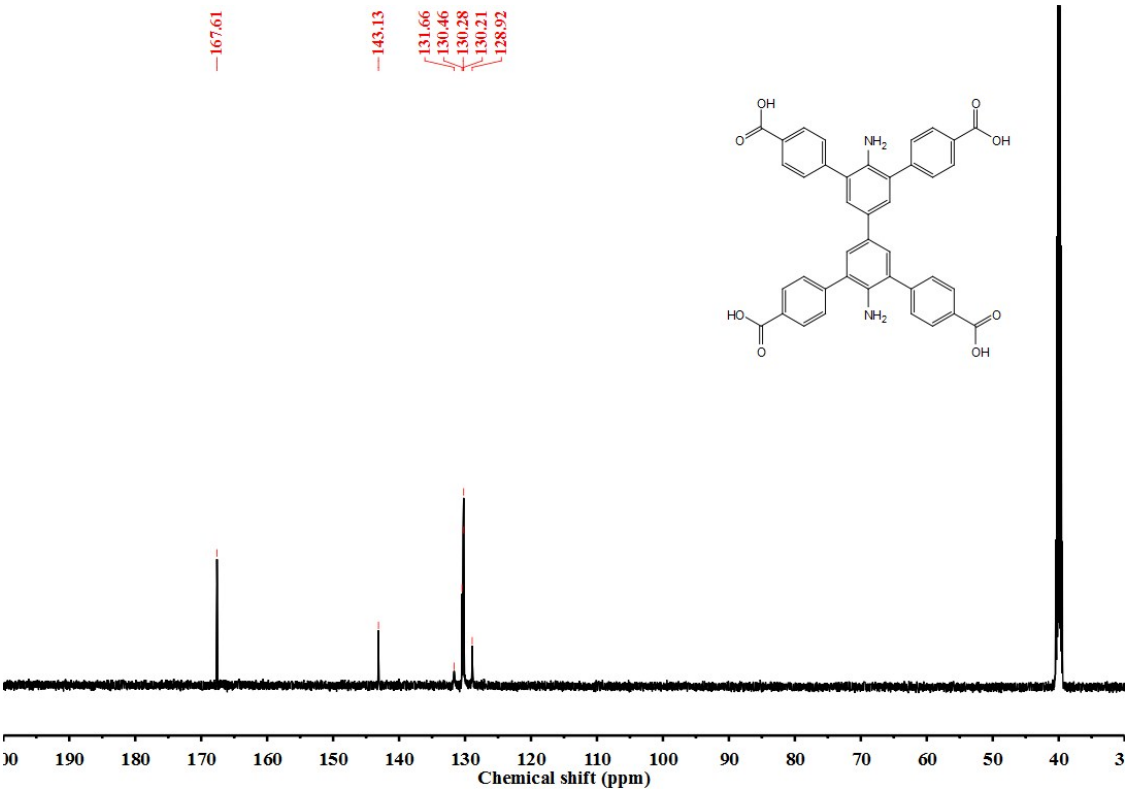

Figure S2. ^{13}C (DMSO-d_6, 500MHz) spectra of the ligand H_4L.

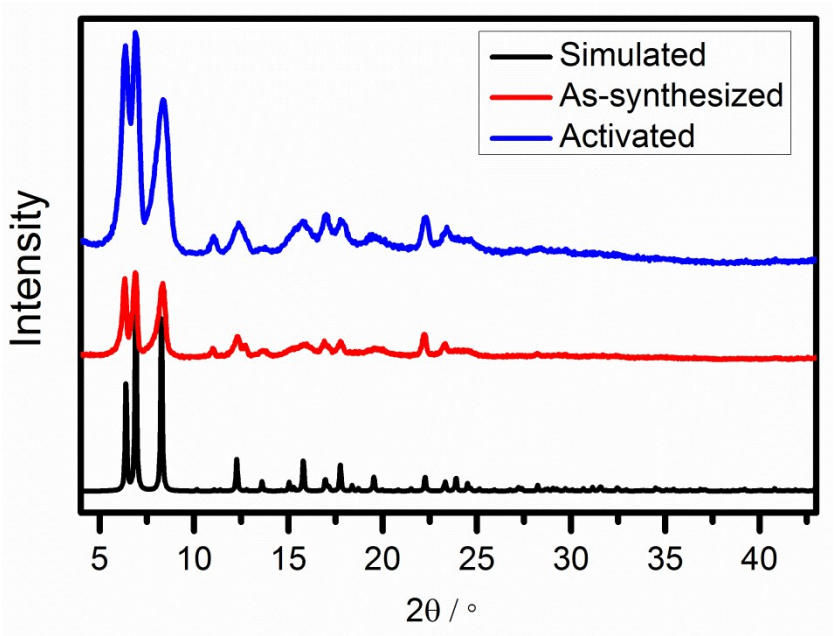

Figure S3. PXRD patterns of as-synthesized UTSA-67 (red) and activated UTSA-67a (blue) along with the simulated XRD pattern from the single-crystal X-ray structure (black).

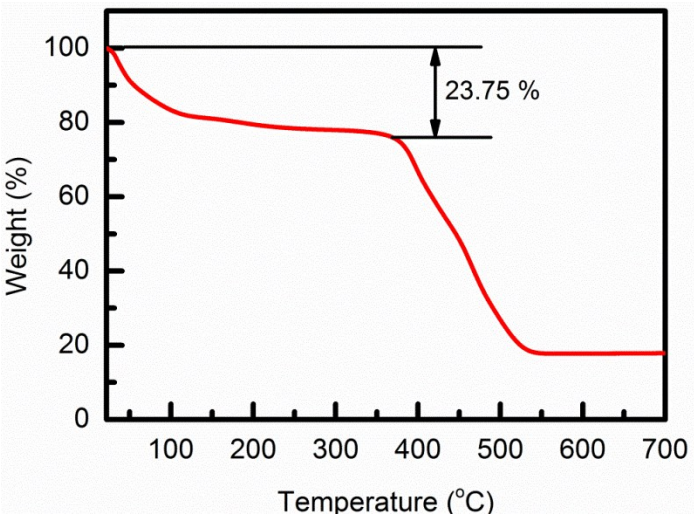

Figure S4. TGA curves of as–synthesized UTSA-67.

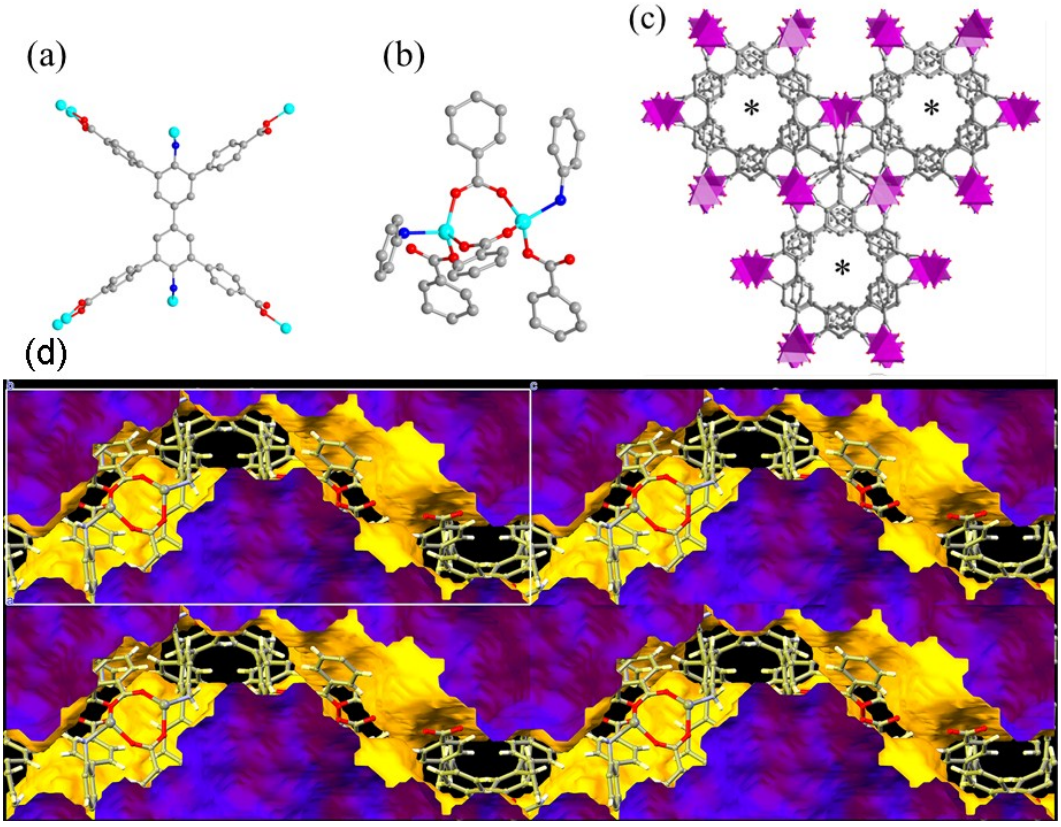

Figure S5. X-ray single crystal structure of UTSA-67: (a) coordination modes of carboxylate and amino groups in the organic linker; (b) the coordination environment of the binuclear zinc cluster; (c) the pore channels viewed along the *c* axes. The symbols of * represent the 6-fold screw axes. (d) the one-dimensional channel along the *c* axes.

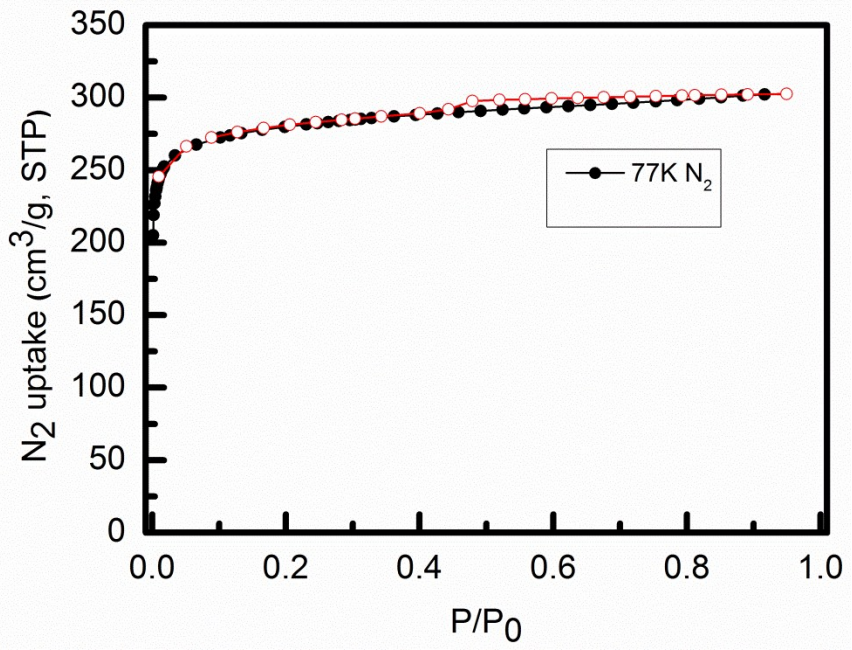

Figure S6. N_2 sorption isotherms of UTSA-67a at 77 K. Closed symbols, adsorption; open symbols, desorption.

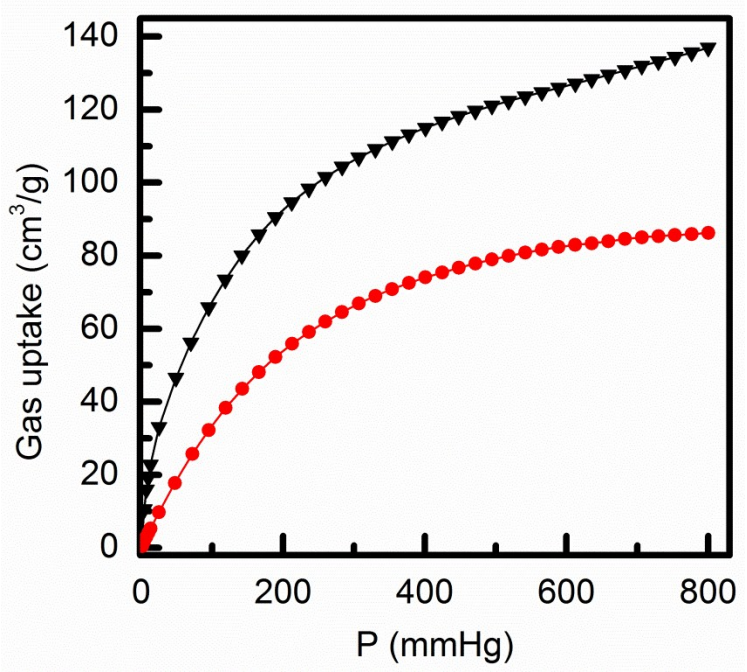

Figure S7. Single-component adsorption isotherms for C_2H_2 (black) and C_2H_4 (red) of UTSA-67a at 273 K.

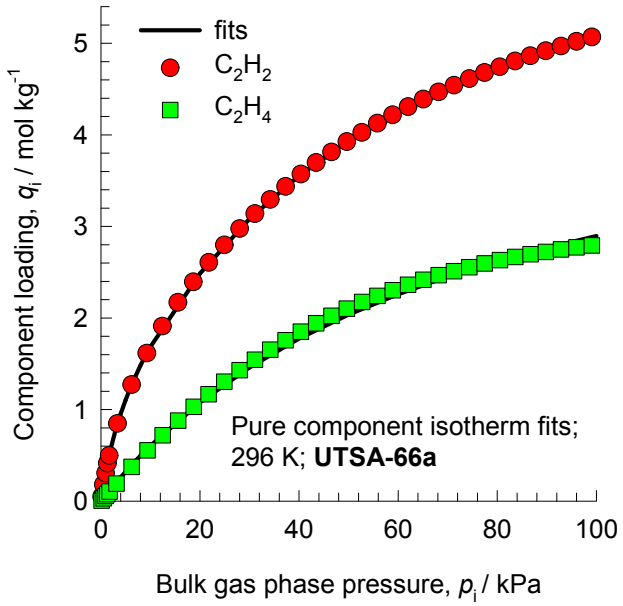

Figure S8. Comparison of component loadings for C_2H_2, and C_2H_4 at 296 K in UTSA-67a with the dual-Langmuir-Freundlich isotherm fits.

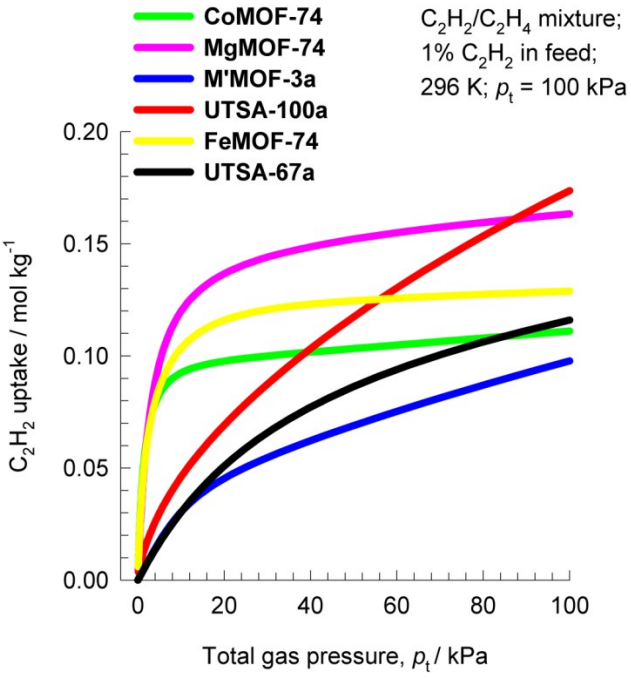

Figure S9. IAST calculations of the uptake capacity of C_2H_2 for adsorption from C_2H_2/C_2H_4 mixtures containing 1% C_2H_2. The partial pressures of C_2H_2, and C_2H_4 are, respectively, p_1 = 1 kPa, p_2 = 99 kPa at T = 296 K. The data for FeMOF-74 is at a temperature of 318 K; this is the lowest temperature used in the isotherm measurements of Bloch et al.[9]

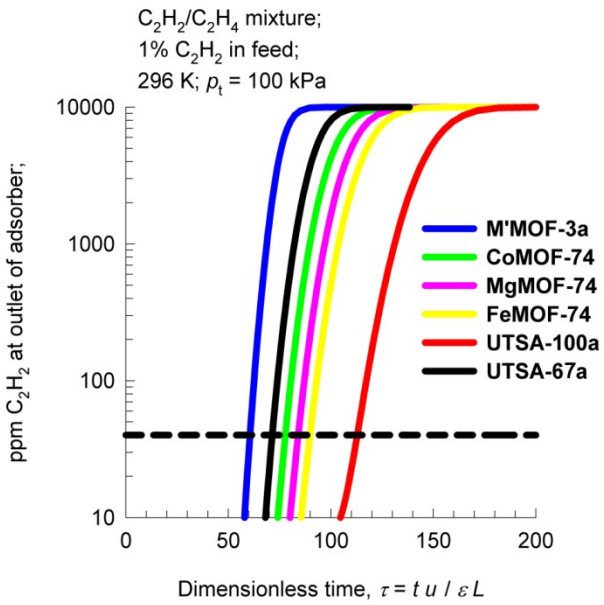

Figure S10. Ppm C_2H_2 in the outlet gas of an adsorber bed packed with UTSA-67a, MgMOF-74, CoMOF-74, FeMOF-74, M'MOF-3a, and UTSA-100a. The total bulk gas phase is 100 kPa; the partial pressures of C_2H_2, and C_2H_4 in the inlet feed gas mixture are, respectively, p_1 = 1 kPa, p_2 = 99 kPa. The temperature is 296 K for all MOFs except FeMOF-74 for which the chosen temperature is 318 K.[9]

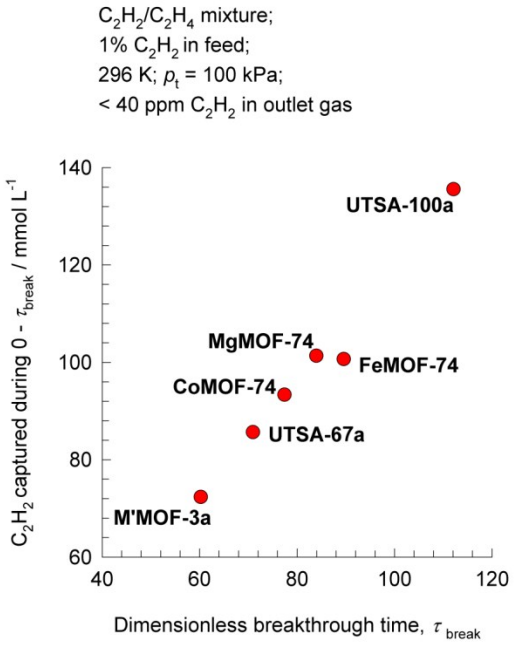

Figure S11. Plot of C_2H_2 captured per L of adsorbent, during the time interval $0-\tau_{break}$, plotted as a function of the time interval τ_{break}. The temperature is 296 K for all MOFs except for FeMOF-74 for which the chosen temperature is 318 K.

Table S1. Crystallographic data and structure refinement results for UTSA-67 (from single-crystal X-ray diffraction analysis on the as-synthesized sample).

	UTSA-67
Formula	$C_{40}H_{24}N_2Zn_2O_{11}$
Formula weight	839.39
Temperature/K	293.00(19)
Crystal system	hexagonal
Space group	P6522
a (Å)	15.9684(5)
b (Å)	15.9684(5)
c (Å)	33.649(4)
α (°)	90.00
β (°)	90.00
γ (°)	120.00
V (Å^3)	7430.6(9)
Z	12
D_{calcd} (g cm^{-3})	1.0572
μ (mm^{-1})	1.017
F(000)	2556.0
Crystal size/mm^3	0.30 × 0.20 × 0.20
GOF	1.070
R_{int}	0.0816
R_1, wR_2 [I>=2σ (I)]	0.1139, 0.2978
R_1, wR_2 [all data]	0.1616, 0.3341
Largest diff. peak and hole (e Å^{-3})	0.874, -0.675

Table S2. Dual-Langmuir-Freundlich parameter fits for UTSA-67a.

	Site A				Site B			
	$q_{A,sat}$ mol kg^{-1}	b_{A0} $Pa^{-\nu_i}$	E_A kJ mol^{-1}	ν_A dimensionless	$q_{B,sat}$ mol kg^{-1}	b_{B0} $Pa^{-\nu_i}$	E_B kJ mol^{-1}	ν_B dimensionless
C_2H_2	1.7	3.07×10^{-10}	33	1.25	5.2	5.46×10^{-11}	25	1
C_2H_4	5	2.56×10^{-10}	26.8	1				

Table S3. Comparison of some microporous MOFs for C_2H_2/C_2H_4 separation at room temperature.

	UTSA-67a	M'MOF-3a	CoMOF-74	MgMOF-74	FeMOF-74	NOTT-300	UTSA-100a	UTSA-60a
Surface area ($m^2\ g^{-1}$)[a]	1136.7	110	1018	927	1350	1370	970	484
Pore volume ($cm^3\ g^{-1}$)	0.47	0.165	0.515	0.607	0.626	0.433	0.399	0.189
Size of pore window (Å)	3.3×3.3	3.4×4.8	11×11	11×11	11×11	6.5×6.5	4.3×4.3	4.8×4.0
C_2H_2 uptake (mmol g^{-1})	5.13	1.90	8.17	8.37	6.80[b]	6.34[c]	4.27	3.12
C_2H_4 uptake (mmol g^{-1})	2.81	0.40	7.02	7.45	6.10[b]	4.28[c]	1.66	2.05
C_2H_2/C_2H_4 uptake ratio	1.84	4.75	1.16	1.12	1.11	1.48	2.57	1.52
Selectivity[d]	5–6	24.03	1.70	2.18	2.08	2.17	5–10.7	5.5–16
Q_{st} (C_2H_2, kJ mol^{-1})[e]	32	25	45	41	46	32	22	36
Ref.	This work	8	8	8	9	5	5	4

[a] BET. [b] At temperature of 318 K. [c] At temperature of 293 K. [d] IAST analysis for C_2H_2/C_2H_4 mixtures containing 1% acetylene at 100 kPa. [e] The initial Q_{st} values.

Table 4. Breakthrough calculations for separation of C_2H_2/C_2H_4 mixture containing 1 mol% C_2H_2 at 296 K. The data for FeMOF-74 is at a temperature of 318 K; this is the lowest temperature used in the isotherm measurements of Bloch et al.[9] The product gas stream contains less than 40 ppm C_2H_2.

MOFs	Dimensionless breakthrough time τ_{break}	C_2H_2 adsorbed during 0 - τ_{break} mmol L^{-1}	Ref.
CoMOF-74	77.4	93.3	8
MgMOF-74	84	101.3	8
FeMOF-74	89.6	100.7	8
UTSA-100a	112	135.5	5
M'MOF-3a	60.2	72.3	8
NOTT-300	56.2	68.3	5
UTSA-60a	55	52	4
UTSA-67a	70.9	85.7	This work

References

1. Wehrmann, P. and Mecking S., *Organometallics*, 2008, **27**, 1399–1408.

2. Sheldrick, G. M. Program for Structure Refinement. Germany, **1997**.

3. Spek, L. PLATON: The University of Utrecht: Utrecht, The Netherlands, **1999**.

4. H.-M. Wen, B. Li, H. Wang, C. Wu, K. Alfooty, R. Krishnad and B. Chen, *Chem. Commun.*, 2015, **51**, 5610–5613.

4. A. L. Myers and J. M. Prausnitz, *A.I.Ch.E.J.*, 1965, **11**, 121–127.

5. T.-L. Hu, H. Wang, B. Li, R. Krishna, H. Wu, W. Zhou, Y. Zhao, Y. Han, X. Wang, W. Zhu, Z. Yao, S. Xiang and B. Chen, *Nat. Commun.*, 2015, **6**, 7328.

6. R. Krishna and J. R. Long, *J. Phys. Chem. C*, 2011, **115**, 12941–12950.

7. R. Krishna, *Microporous Mesoporous Mater.*, 2014, **185**, 30–50.

8. Y. He, R. Krishna and B. Chen, *Energy Environ. Sci.*, 2012, **5**, 9107–9120.

9. E. D. Bloch, W. L. Queen, R. Krishna, J. M. Zadrozny, C. M. Brown and J. R. Long, *Science*, 2012, **335**, 1606–1610.